Trajectory Tracking Motion Control System for Observation Class ROVs

Daniel de A. Fernandes * **Asgeir J. Sørensen** *
Décio C. Donha **

* *Centre for Autonomous Marine Operations and Systems (AMOS) – Dept. of Marine Technology – Norwegian Univ. of Science and Tech. (NTNU) – Trondheim, Norway (e-mail: daniel.fernandes@ntnu.no; dalmeidafernandes@gmail.com; asgeir.sorensen@ntnu.no)*
** *University of São Paulo (USP) – São Paulo, Brazil – Dept. of Mechanical Engineering (e-mail: decdonha@usp.br)*

Abstract: This paper proposes a MCS (Motion Control System) with trajectory tracking capability for observation class ROVs (Remotely Operated Vehicle) used to carry out automated high-resolution image capturing missions, e.g. inspections, mappings, and surveys. The trajectory tracking capability is a key feature to enable the end users of the ROV technology to acquire sequential high-quality images at proper pace to construct consistent representations of the objects or of the environments of interest. Four degrees-of-freedom are controlled – surge, sway, heave, and yaw. The MCS consists of an output feedback control system that is composed of a high-gain state observer and a MIMO (Multiple-Input-Multiple-Output) PID (Proportional-Integral-Derivative) controller, that works aided by reference feedforward. Plant linearisation is performed aiming at improving the tracking performance. Stability and satisfactory performance of suitable and smooth reference trajectories are attained despite the presence of unmodelled dynamics, plant parameter variations, measurement noise, and environmental disturbances. Simulated results based on the model of the NTNU's ROV Minerva are presented.

Keywords: Feedback Linearisation, High-Gain State Observer, MIMO PID Control, Nonlinear Control, Output Feedback Control, Remotely Operated Vehicle, Tracking Control System.

1. INTRODUCTION

Observation class ROVs (Remotely Operated Vehicle) are used worldwide as carriers of imagery devices, e.g. cameras, sonars, echo sounders, hyperspectral imagers, for industrial, military, and research activities, such as inspection, mapping, and survey, see Christ and Wernli (2007), Ludvigsen et al. (2007), Marsh et al. (2013), Singh et al. (2007), and references therein. ROVs are typically fully-actuated vehicles with open-frame structures, operated from support vessels through umbilical cables transmitting power, commands, and data. MCSs (Motion Control System) for ROVs are typically composed of navigation, guidance, and control systems. The navigation system determines the state variables, by means of direct measurement or reconstruction via state estimation. It can also determine other quantities, e.g. battery charge level, and detect faults, e.g. malfunctioning propellers, in order to secure operation safety and reliability. The guidance system generates feasible and smooth reference trajectories. It concerns the transient motion behaviour associated with the achievement of the motion control objectives. The control system provides the necessary propulsion and steering forces and moments so the reference trajectories can be tracked by the ROVs. Regardless of the type of mission that is carried out, accurate motion control is always required for capturing images in order to construct consistent representations of objects or of environments of interest.

Therefore, it is proposed in this paper a MCS with tracking capability for observation class ROVs. It consists of an output feedback control system that is composed of a HGSO (High-Gain State Observer) and a MIMO (Multiple-Input-Multiple-Output) PID (Proportional-Integral-Derivative) controller, that works aided by reference feedforward for improved performance. Plant linearisation is also performed to help the reference trajectory tracking task. The MCS requires the measurement of the position and heading of the ROVs. The HGSO behaves approximately like a differentiator (Khalil, 2002), thus fitting this application where velocities are not directly measured, but are obtained from noisy position and attitude measurements. The HGSO is found to be relatively easier to tune, as a single-parameter-tuning state observer, than the benchmark EKF (Extended Kalman Filter) tested earlier on the ROV Minerva (Sørensen et al., 2012). Additionally, its machine code requires less memory space to be stored and is faster to be run than the EKF, which is advantageous if a microcontroller-based embedded control system is considered instead of a computationally more complex and powerful microprocessor-based system. The reference model found in Fernandes et al. (2012) is used in this work to generate the reference trajectories for the guided motions.

Stability and satisfactory performance are expected from the MCS, although it relies upon the CPM (Control Plant Model) (Sørensen, 2013), which is a simplified descrip-

tion of the actual plants of the ROVs, whose parameters change over time mostly depending on operational and environmental conditions. Besides, ROVs and their umbilical cables are subject to disturbing forces caused by the sea current. The performance of the proposed MCS is demonstrated by simulation results based on the NTNU's ROV Minerva. Such results emphasise the value of the HGSO for this application and shed light on the problem of accurately controlling ROVs by using a low fidelity CPM.

This work is inspired by the works by Khalil (2002), Esfandiari and Khalil (1992), and Atassi and Khalil (2000), where observed-based robust controllers are designed to stabilise fully linearisable nonlinear systems, given that they are left-invertible and minimum-phase. According to these authors, the HGSO has the ability to robustly estimate the unmeasured states, while asymptotically attenuating disturbances. Perrier and Canudas-de-Wit (1996) presented an approach for designing simple nonlinear robust controllers for underwater vehicles. They explored the potentiality of bridging linear and nonlinear control techniques, by associating nonlinear controllers with the classical PID controller, to improve the systems' stability and disturbance rejection properties. In this paper, in contrast with the mentioned work, full state feedback is provided for the sake of enhanced motion control.

The paper is organised as follows. Section 2 introduces the CPM of the ROVs. Sections 3 and 4 concern the control and navigation systems of the MCS. Section 5 presents simulation results. Section 6 presents concluding remarks. Appendix A introduces the NTNU's ROV Minerva.

2. CONTROL PLANT MODEL

The CPM follows the nomenclature defined by SNAME (1950). It is based on the models found in Fossen (2011) and Sørensen (2013). It is built on the following premisses: i) the ROV is fully actuated in its 4-DoF configuration space (Breivik and Fossen, 2009) – surge, sway, heave, and yaw motions; ii) the remaining DoFs are self-stable by the design of the ROV; iii) the locations of the CG (Centre of Gravity) and the CB (Centre of Buoyancy) are fixed; iv) the ROV operates below the wave-affected zone; v) the velocity and orientation of the sea current vary slowly enough to be taken as constant; and vi) the fluid is irrotational, of constant density, and of infinite extent. Its explicit dependence on time is omitted for the sake of better readability.

The control plant model is given by

$$\begin{cases} \dot{\boldsymbol{\eta}} = \boldsymbol{J}(\psi)\,\boldsymbol{\nu} \\ \boldsymbol{M}\,\dot{\boldsymbol{\nu}} = -\,\boldsymbol{C}(\boldsymbol{\nu})\,\boldsymbol{\nu} - \boldsymbol{D_L}\,\boldsymbol{\nu} - \boldsymbol{D_Q}\;|\boldsymbol{\nu}|\boldsymbol{\nu} + \boldsymbol{g} + \boldsymbol{c} + \boldsymbol{\tau} \end{cases} \tag{1}$$

where $\boldsymbol{J}(\psi) \in SO(4)$ (Special Orthogonal group of order 4) is a transformation matrix transforming the relative velocity vector $\boldsymbol{\nu} = [u, v, w, r]^T$, that is given in the BF (Body-Fixed) coordinate frame, into the 'absolute' velocity vector $\dot{\boldsymbol{\eta}} = [\dot{n}, \dot{e}, \dot{d}, \dot{\psi}]^T$, that is given in the 'inertial' NED (North-East-Down) coordinate frame. The position and attitude vector $\boldsymbol{\eta} = [n, e, d, \psi]^T$ gives the position from the chosen origin of the NED frame, and the heading angle with respect to the N-axis of the NED frame. The inertia matrix $\boldsymbol{M} \in \mathbb{R}^{4\times4} \,|\, \boldsymbol{M} \triangleq \boldsymbol{M_{RB}} + \boldsymbol{M_A} > 0$ embodies the mass and the inertia tensor of the rigid-body $\left(\boldsymbol{M_{RB}} \in \mathbb{R}^{4\times4} \,|\, \boldsymbol{M_{RB}} > 0\right)$, and the hydrodynamic 'added' masses and the inertia tensor $\left(\boldsymbol{M_A} \in \mathbb{R}^{4\times4} \,|\, \boldsymbol{M_A} \geqslant 0\right)$. The Coriolis-centripetal matrix $\boldsymbol{C}(\boldsymbol{\nu}) \triangleq \boldsymbol{C_{RB}}(\boldsymbol{\nu}) + \boldsymbol{C_A}(\boldsymbol{\nu}) \in SS(4)$ (Skew-Symmetric group of order 4) is straightforwardly derived from $\boldsymbol{M}$. The matrix $\boldsymbol{D_L} \in \mathbb{R}^{4\times4} \,|\, \boldsymbol{D_L} > 0$ collects linear hydrodynamic damping coefficients regarding linear skin friction (laminar flows). The matrix $\boldsymbol{D_Q} \in \mathbb{R}^{4\times4} \,|\, \boldsymbol{D_Q} > 0$ collects quadratic hydrodynamic damping coefficients regarding quadratic skin friction and vortex shedding (turbulent flows). All elements (hydrodynamic derivatives) of $\boldsymbol{M}$, $\boldsymbol{D_L}$, and $\boldsymbol{D_Q}$ are expected to be nonzero and distinct, as the ROV has an open-frame structure with asymmetries in the shapes and distribution of its internal parts and components. Besides, every element of these matrices may split into a pair of relatively close values regarding positive and negative velocities for each DoF, and may yet vary about the nominal values (Caccia et al., 2000; Lewandowski, 2004). The factors affecting $\boldsymbol{M}$ naturally affect $\boldsymbol{C}(\boldsymbol{\nu})$. The vector of signed squares $|\boldsymbol{\nu}|\boldsymbol{\nu} \triangleq [|u|u, |v|v, |w|w, |r|r]^T$ represents quadratic relative velocities. The vector of hydrostatic restoring forces $\boldsymbol{g} = [0, 0, (W-B), 0]^T$ collects the weight force $W = m\,g$ acting upon the CG, and the buoyancy force $B = \rho\,\nabla\,g$ acting upon the CB, where m is the ROV's (dry) mass, g is the acceleration of gravity, ρ is the fluid density, and ∇ is the total volume of fluid displaced by the ROV. It is safer to have an ROV designed slightly positive buoyant, that is, $|B| > W$, since it can emerge to the surface in case a hard failure occurs in the MCS. The vector $\boldsymbol{c} \in \mathbb{R}^4$ represents unmeasured (nonestimated either) current-generated perturbing forces and moment, since the speed and direction of the sea current are not measured or estimated in this work. Notice that (1) is based only on body-fixed velocities, without taking the current velocities into account, since their effects are collected into $\boldsymbol{c}$. The vector $\boldsymbol{\tau} \in \mathbb{R}^4$ represents the propulsion and steering forces and moment delivered by the propulsion system (left unmodelled).

3. CONTROL SYSTEM

3.1 Introduction

The control system performs two tasks: i) linearisation of the dynamics of the CPM; and ii) asymptotic tracking of the reference vector $\left[\boldsymbol{\eta_R}^T, \boldsymbol{\nu_R}^T\right]^T \in \mathbb{R}^8$. The first task is performed aiming at helping the performance of the second task. The linearisation also allows the use of a linear state observer, such as the HGSO, to estimate the unmeasured states (velocities) and filter the measured states (position and heading) of (1). The HGSO is treated in Section 4.

3.2 Separation Principle

It is assumed throughout Section 3 that the state vector $\left[\boldsymbol{\eta}^T, \boldsymbol{\nu}^T\right]^T \in \mathbb{R}^8$ is available for feedback as if measured. This assumption is supported by the separation principle (Khalil, 2002; Esfandiari and Khalil, 1992; Atassi and Khalil, 2000), which holds for this MCS, provided that (1) can be proved to be left-invertible and minimum-phase. The CPM has both properties if its linearised version also has them (Esfandiari and Khalil, 1992). The left-inversion problem characterises structural properties of a model regarding state estimation and reconstruction (Estrada et

al., 2007). Perfect asymptotic tracking cannot be achieved by a nonminimum-phase system (Slotine and Li, 2005).

The nonlinear terms $\boldsymbol{C}(\boldsymbol{\nu})\,\boldsymbol{\nu}$ and $\boldsymbol{D_Q}\,|\boldsymbol{\nu}|\boldsymbol{\nu}$ in the dynamics of (1) could theoretically be cancelled out by state feedback, as both satisfy the matching condition, that is, they enter the dynamics at the same point the input vector $\boldsymbol{\tau}$ does (Khalil, 2002). The vector $\boldsymbol{g}$ also satisfies the matching condition, and could theoretically be eliminated from (1), if properly counteracted by $\boldsymbol{\tau}$. As a consequence of getting rid of all these three terms, as detailed within Subsection 3.3, the CPM could be represented by the following NTV (Nonlinear and Time-Varying) state-space model

$$\begin{cases} \dot{\boldsymbol{x}} = \boldsymbol{A}(\psi)\,\boldsymbol{x} + \boldsymbol{B}\,(\boldsymbol{c}+\boldsymbol{\tau}) \\ \boldsymbol{y} = \boldsymbol{C}\,\boldsymbol{x} \end{cases} \tag{2}$$

where $\boldsymbol{x} \triangleq \left[\boldsymbol{\eta}^T, \boldsymbol{\nu}^T\right]^T$ is the state vector and $\boldsymbol{y} \triangleq \boldsymbol{\eta}$ is the output vector. The vectors $\boldsymbol{c}$ and $\boldsymbol{\tau}$ are the same as in (1), where $\boldsymbol{\tau}$ is the control vector. The matrices are defined as

$$\boldsymbol{A}(\psi) \triangleq \begin{bmatrix} \boldsymbol{0} & \boldsymbol{J}(\psi) \\ \boldsymbol{0} & -\boldsymbol{M}^{-1}\boldsymbol{D_L} \end{bmatrix}, \quad \boldsymbol{B} \triangleq \begin{bmatrix} \boldsymbol{0} \\ \boldsymbol{M}^{-1} \end{bmatrix}, \quad \boldsymbol{C} \triangleq [\boldsymbol{I} \quad \boldsymbol{0}] \tag{3}$$

where $\boldsymbol{0}, \boldsymbol{I} \in \mathbb{R}^{4\times 4}$ are the null and identity matrices.

Consider the LTI (Linear and Time-Invariant) (Jacobian) matrix $\boldsymbol{A} \in \mathbb{R}^{8\times 8} | \boldsymbol{A} \triangleq \frac{\partial}{\partial \boldsymbol{x}}[\boldsymbol{f}(\boldsymbol{x})]|_{\boldsymbol{x_0}\equiv\boldsymbol{0}}$, where $\boldsymbol{x_0}$ is the state at which the NTV function $\boldsymbol{f}(\boldsymbol{x}) \triangleq \boldsymbol{A}(\psi)\,\boldsymbol{x}$ in (2) is linearised. Then, the LTI system described by the matrix triple $(\boldsymbol{A}, \boldsymbol{B}, \boldsymbol{C})$ is: i) a minimal realisation, as it has no transmission zeros in the complex plane s, and hence it is minimum-phase; and ii) is left-invertible, since the transfer function matrix $\boldsymbol{T}(s) \triangleq \boldsymbol{C}\,(s\boldsymbol{I}-\boldsymbol{A})^{-1}\boldsymbol{B} \in \mathbb{R}^{4\times 4}$ has full rank $\forall\, s \in \mathbb{C}$. Equivalently, $\dim(\ker(\boldsymbol{T}(s))) = 0\,\forall\, s \in \mathbb{C}$. The pair $(\boldsymbol{A}, \boldsymbol{B})$ is controllable, as the controllability matrix $\mathcal{C}$ has full row rank, given that $\det(\mathcal{C}) = \det\left(\boldsymbol{M}^{-2}\right)$, and the pair $(\boldsymbol{A}, \boldsymbol{C})$ is observable, as the observability matrix $\mathcal{O}$ has full column rank, given that $\det(\mathcal{O}) = 1$. Details on such properties of LTI systems can be found in Franklin et al. (2009), Estrada et al. (2007), Kailath (1980), Khalil (2002), and Slotine and Li (2005). The purely kinematic nonlinearity $\boldsymbol{J}(\psi)$ does not affect the constant eigenvalues of $\boldsymbol{A}(\psi)$, denoted $\lambda_i(\boldsymbol{A}(\psi)) \equiv \lambda_i(\boldsymbol{A})$, $i \in \mathbb{N} \,|\, i \in \{1, \ldots, 8\}$, $\forall\, \psi \in \mathbb{R}$, as the eigenvalues of the matrices $\boldsymbol{A}(\psi)$ and $\boldsymbol{A}$ are the roots of the common 8th-order characteristic equation $\det(s\boldsymbol{I})\det\left(s\boldsymbol{I}+\boldsymbol{M}^{-1}\boldsymbol{D_L}\right) = 0$, due to their upper-triangular structures. The matrix pairs $(\boldsymbol{A}(\psi), \boldsymbol{B})$ and $(\boldsymbol{A}(\psi), \boldsymbol{C})$ can be shown to be controllable and observable, respectively, $\forall\, \psi \in \mathbb{R}$, by the use of Lie brackets and Lie derivatives (Khalil, 2002; Slotine and Li, 2005).

3.3 Control Vector

The control loop is closed as the control vector $\boldsymbol{u}$ is applied to the input of (1), that is, by imposing that $\boldsymbol{\tau} = \boldsymbol{u}$. The control vector is defined in this work as

$$\boldsymbol{u} \triangleq \boldsymbol{u_{LIN}} + \boldsymbol{u_{PID}} + \boldsymbol{u_{FF}} \tag{4}$$

where $\boldsymbol{u_{LIN}}$ tackles to cancel out the nonlinearities in the dynamics of (1) discussed in Subsection 3.2, $\boldsymbol{u_{PID}}$ provides full state feedback, and $\boldsymbol{u_{FF}}$ provides reference feedforward. All terms are going to be detailed in the sequence.

Linearisation of the dynamics of the CPM: The linearisation term is defined as

$$\boldsymbol{u_{LIN}} \triangleq \overline{\boldsymbol{C}(\boldsymbol{\nu})}\,\boldsymbol{\nu} + \overline{\boldsymbol{D_Q}}\,|\boldsymbol{\nu}|\boldsymbol{\nu} - \overline{\boldsymbol{g}} \tag{5}$$

where $\overline{\boldsymbol{C}(\boldsymbol{\nu})}$, $\overline{\boldsymbol{D_Q}}$, and $\overline{\boldsymbol{g}}$ are the nominal expressions of $\boldsymbol{C}(\boldsymbol{\nu})$, $\boldsymbol{D_Q}$, and $\boldsymbol{g}$ to be implemented in the MCS. The nominal matrices $\overline{\boldsymbol{C}(\boldsymbol{\nu})}$ and $\overline{\boldsymbol{D_Q}}$ may differ from their actual counterparts, as $\overline{\boldsymbol{C}(\boldsymbol{\nu})}$ and $\overline{\boldsymbol{D_Q}}$ have fixed entries, whereas both actual matrices may vary during operation, see Section 2. The nominal matrices often have diagonal structures, because it is difficult to obtain accurate estimates of their nondiagonal elements (Caccia et al., 2000; Fossen, 2011; Lewandowski, 2004; Sørensen, 2013). The vector $\overline{\boldsymbol{g}}$ may also slightly differ from the actual $\boldsymbol{g}$. The vector $\boldsymbol{u_{LIN}}$ represents the best endeavour towards linearising the dynamics of the CPM. However, the nonlinearities can never be exactly cancelled out, because the CPM always contains some modelling simplifications and uncertainties.

Asymptotic trajectory tracking: The objective is to achieve $\|\boldsymbol{\eta_R} - \boldsymbol{\eta}\| \to 0$ and $\|\boldsymbol{\nu_R} - \boldsymbol{\nu}\| \to 0$, as $t \to \infty$, where $\boldsymbol{\eta_R} = \boldsymbol{\eta_R}(t) \in \mathbb{R}^4$, $\boldsymbol{\nu_R} = \boldsymbol{\nu_R}(t) \in \mathbb{R}^4$, and $t \in [0, \infty)$ is the time. Notice that $\boldsymbol{\nu_R}(t) \triangleq \boldsymbol{J}^T(\psi_R)\,\frac{\mathrm{d}}{\mathrm{d}t}[\boldsymbol{\eta_R}(t)]$. This task is performed by a MIMO PID controller and by the anticipative action provided by reference feedforward. PIDs fit well applications where sufficiently damped 2nd-order dynamics are dealt with (Åström and Hägglund, 2011). A number of successful applications based on PIDs can be found in literature (Breivik and Fossen, 2009; Fernandes et al., 2012; Fossen, 2011; Perrier and Canudas-de-Wit, 1996; Sørensen, 2013; Sørensen et al., 2012, and references therein). Asymptotic tracking requires feedforward action to ensure that the needed control effort to achieve the goal is provided (Franklin et al., 2009; Slotine and Li, 2005).

The feedback term is defined as

$$\boldsymbol{u_{PID}} \triangleq \boldsymbol{K_P}\,\boldsymbol{J}^T(\psi)\,\boldsymbol{e_\eta} + \boldsymbol{K_I}\,\boldsymbol{J}^T(\psi)\,\boldsymbol{e_I} + \boldsymbol{K_D}\,\boldsymbol{e_\nu} \tag{6}$$

where $\boldsymbol{e_t} \triangleq \left[\boldsymbol{e_I}^T, \boldsymbol{e_\eta}^T, \boldsymbol{e_\nu}^T\right]^T$ is the tracking error vector, whose components are the position tracking error vector $\boldsymbol{e_\eta} \triangleq \boldsymbol{\eta_R} - \boldsymbol{\eta}$, the velocity tracking error vector $\boldsymbol{e_\nu} \triangleq \boldsymbol{\nu_R} - \boldsymbol{\nu}$, and the integral of $\boldsymbol{e_\eta}$ evaluated over time $\boldsymbol{e_I} \triangleq \int_0^t \boldsymbol{e_\eta}(\tau)\,d\tau$. The diagonal matrices $\boldsymbol{K_P}, \boldsymbol{K_I}, \boldsymbol{K_D} \in \mathbb{R}^{4\times 4} \,|\, \boldsymbol{K_P}, \boldsymbol{K_I}, \boldsymbol{K_D} > 0$ are assigned the proportional, integral, and derivative gain sets of the MIMO PID controller.

The reference feedforward term is defined as

$$\boldsymbol{u_{FF}} \triangleq \overline{\boldsymbol{D_L}}\,\boldsymbol{\nu_R} + \overline{\boldsymbol{M}}\,\dot{\boldsymbol{\nu}}_{\boldsymbol{R}} \tag{7}$$

where $\overline{\boldsymbol{D_L}}$ and $\overline{\boldsymbol{M}}$ are the nominal expressions of $\boldsymbol{D_L}$ and $\boldsymbol{M}$ to be implemented in the MCS. The nominal matrices $\overline{\boldsymbol{D_L}}$ and $\overline{\boldsymbol{M}}$ may differ from their actual counterparts, since $\overline{\boldsymbol{D_L}}$ and $\overline{\boldsymbol{M}}$ have fixed entries, whereas the actual matrices may vary during operation, see Section 2. Both nominal matrices often have diagonal structures, because it is difficult to obtain accurate estimates of their nondiagonal elements (Caccia et al., 2000; Fossen, 2011; Lewandowski, 2004; Sørensen, 2013).

3.4 Tracking Error Dynamics

By substituting the terms (5)–(7) into (4), and then by substituting the resulting expression (4) into (1) (imposing that $\boldsymbol{\tau} = \boldsymbol{u}$), and lastly by performing a few algebraic operations to the finally obtained expression, the tracking error dynamics turns out to be given by

$$\dot{\boldsymbol{e}}_{\boldsymbol{t}} = \boldsymbol{A}_{\boldsymbol{t}}(\psi)\, \boldsymbol{e}_{\boldsymbol{t}} + \boldsymbol{B}_{\boldsymbol{t}}\, \boldsymbol{\delta}(\boldsymbol{\nu}) + \boldsymbol{B}_{\boldsymbol{R}} \left[\boldsymbol{\nu}_{\boldsymbol{R}}^T, \dot{\boldsymbol{\nu}}_{\boldsymbol{R}}^T\right]^T + \boldsymbol{B}_{\boldsymbol{t}}\, \boldsymbol{c} \tag{8}$$

where

$$\boldsymbol{A}_{\boldsymbol{t}}(\psi) = \begin{bmatrix} \boldsymbol{0} & \boldsymbol{I} & \boldsymbol{0} \\ \boldsymbol{0} & \boldsymbol{0} & \boldsymbol{J}(\psi) \\ \boldsymbol{A}_{\boldsymbol{t}_{31}}(\psi) & \boldsymbol{A}_{\boldsymbol{t}_{32}}(\psi) & \boldsymbol{A}_{\boldsymbol{t}_{33}} \end{bmatrix} \tag{9}$$

$$\boldsymbol{A}_{\boldsymbol{t}_{31}}(\psi) = -\boldsymbol{M}^{-1}\, \boldsymbol{K}_{\boldsymbol{I}}\, \boldsymbol{J}^T(\psi) \tag{10}$$

$$\boldsymbol{A}_{\boldsymbol{t}_{32}}(\psi) = -\boldsymbol{M}^{-1}\, \boldsymbol{K}_{\boldsymbol{P}}\, \boldsymbol{J}^T(\psi) \tag{11}$$

$$\boldsymbol{A}_{\boldsymbol{t}_{33}} = -\boldsymbol{M}^{-1} \left(\boldsymbol{D}_{\boldsymbol{L}} + \boldsymbol{K}_{\boldsymbol{D}}\right) \tag{12}$$

$$\boldsymbol{B}_{\boldsymbol{t}} = \begin{bmatrix} \boldsymbol{0} & \boldsymbol{0} & -\boldsymbol{M}^{-T} \end{bmatrix}^T \tag{13}$$

$$\boldsymbol{B}_{\boldsymbol{R}} = \begin{bmatrix} \boldsymbol{0} & \boldsymbol{0} \\ \boldsymbol{0} & \boldsymbol{0} \\ \boldsymbol{M}^{-1}\left(\boldsymbol{D}_{\boldsymbol{L}} - \overline{\boldsymbol{D}_{\boldsymbol{L}}}\right) & \boldsymbol{I} - \boldsymbol{M}^{-1}\overline{\boldsymbol{M}} \end{bmatrix} \tag{14}$$

where $\boldsymbol{0}, \boldsymbol{I} \in \mathbb{R}^{4\times 4}$ are the null and identity matrices, and $\boldsymbol{\delta}(\boldsymbol{\nu})$ lumps together the mismatches which stem from the attempt to linearise the dynamics of (1), such that

$$\boldsymbol{\delta}(\boldsymbol{\nu}) \triangleq \left[\overline{\boldsymbol{C}(\boldsymbol{\nu})} - \boldsymbol{C}(\boldsymbol{\nu})\right]\boldsymbol{\nu} + \left[\overline{\boldsymbol{D}_{\boldsymbol{Q}}} - \boldsymbol{D}_{\boldsymbol{Q}}\right]|\boldsymbol{\nu}|\boldsymbol{\nu} \tag{15}$$

Notice that if the parameters of the CPM could be exactly known, the mismatch term $\boldsymbol{\delta}(\boldsymbol{\nu})$ and the reference input matrix $\boldsymbol{B}_{\boldsymbol{R}}$ would then be both null. It is assumed that the restoring forces are cancelled out, so that $\overline{\boldsymbol{g}} - \boldsymbol{g} \equiv \boldsymbol{0}$. It is also assumed that $\boldsymbol{\delta}(\boldsymbol{\nu})$ remains 'small' enough during the entire ROV operation not to destroy the stability of (8).

The matrix $\boldsymbol{A}_{\boldsymbol{t}}(\psi)$ is NTV. It would be immediate to tune the MIMO PID controller in case it was LTI. Nonetheless, some insight from the physics of the problem helps in that sense. The transformation matrices $\boldsymbol{J}(\psi)$ and $\boldsymbol{J}^T(\psi)$ mutually cancel out each other's effects within $\boldsymbol{A}_{\boldsymbol{t}}(\psi)$, as they appear due to the kinematics of (1), and are unrelated to the dynamics of (1). Consider the global diffeomorphism $\boldsymbol{z} \triangleq \boldsymbol{T}^T(\psi)\, \boldsymbol{e}_{\boldsymbol{t}}$, where $\boldsymbol{T}^T(\psi) \triangleq \text{blockdiag}\big(\boldsymbol{J}^T(\psi), \boldsymbol{J}^T(\psi), \boldsymbol{I}\big)$. The unforced NTV subsystem $\dot{\boldsymbol{e}}_{\boldsymbol{t}} = \boldsymbol{A}_{\boldsymbol{t}}(\psi)\, \boldsymbol{e}_{\boldsymbol{t}}$ of (8) can then be advantageously rewritten as the GES (Globally Exponentially Stable) perturbed LTV (Linear and Time-Varying) system $\dot{\boldsymbol{z}} = \boldsymbol{A}\, \boldsymbol{z} - \boldsymbol{T}^T(\psi)\, \dot{\boldsymbol{T}}(\psi)\, \boldsymbol{z}$ (Slotine and Li, 2005, p. 115), by the use of such global diffeomorphism. The arisen LTI matrix $\boldsymbol{A}$ can be made Hurwitz through proper tuning of the controller, whereas the 'small' sparse skew-symmetric matrix $\boldsymbol{T}^T(\psi)\, \dot{\boldsymbol{T}}(\psi) \to \boldsymbol{0}$, as $t \to \infty$, and $\int_0^\infty \left\| \boldsymbol{T}^T(\psi)\, \dot{\boldsymbol{T}}(\psi) \right\| \mathrm{d}t < \infty$ (the integral exists and is finite $\forall\, t \geqslant 0\,\mathrm{s}$). In particular, the matrix $\boldsymbol{T}^T(\psi)\, \dot{\boldsymbol{T}}(\psi)$ is stable, according to Theorem 4.5 in Khalil (2002, p. 134), and it can be verified that $\boldsymbol{T}^T(\psi)\, \dot{\boldsymbol{T}}(\psi) = \boldsymbol{0}$, whenever $\dot{\psi} = r = 0°/\mathrm{s}$.

Notice that $\boldsymbol{A} \equiv \boldsymbol{A}_{\boldsymbol{t}}(0)$ could also be equivalently obtained by momentarily imposing $\psi = 0° \Rightarrow \boldsymbol{J}(0) = \boldsymbol{J}^T(0) = \boldsymbol{I}$, for tuning purposes. The matrices $\boldsymbol{M}$ and $\boldsymbol{D}_{\boldsymbol{L}}$ in (10)–(12) have to be replaced by $\overline{\boldsymbol{M}}$ and $\overline{\boldsymbol{D}_{\boldsymbol{L}}}$ while the tuning is performed, as the latter matrix pair represents the best of the knowledge about the actual matrices $\boldsymbol{M}$ and $\boldsymbol{D}_{\boldsymbol{L}}$.

4. NAVIGATION SYSTEM

Reconstruction and filtering of the plant states are the tasks of the navigation system, in which a state observer plays the central role. State observers reconstruct the unmeasured plant states in output feedback control systems based on measurements of some state variables (Atassi and Khalil, 2000; Franklin et al., 2009; Kailath, 1980; Khalil, 2002). Moreover, as measurements are often noisy, and may also be jumpy and get frozen awhile, these distortions must be smoothed out prior to supply the output feedback controller (Sørensen, 2013).

In this work a HGSO is used to reconstruct and filter the state vector of the CPM. The section thus focus on an application of the theory found in Khalil (2002), Esfandiari and Khalil (1992), and Atassi and Khalil (2000), where the HGSO is discussed in detail. See Atassi and Khalil (2000) for a discussion about tuning of HGSOs. Shortly recalling its features, the HGSO is a linear system based on the plant model that behaves approximately like a differentiator. It is robust to estimate the unmeasured states, while rejecting the effect of disturbances due to unmodelled dynamics and parameter uncertainties. It allows an output feedback control system to recover its state feedback performance when the observer gains are sufficiently high. Such gains imply much faster poles, and then much faster dynamics, than the closed-loop dynamics of the output feedback control system it is part of, what is in good agreement with the linear state estimation theory (Franklin et al., 2009; Kailath, 1980). It creates high-valued peaks of short duration, proportional to the estimation errors, due to its high gains. The peaking phenomenon is evident at the initial instant ($t = 0\,\mathrm{s}$), when the estimation error is typically larger than during the remaining operating time.

The HGSO is implemented here based on (2), as follows

$$\begin{cases} \dot{\hat{\boldsymbol{x}}} = \overline{\boldsymbol{A}(\psi)}\, \hat{\boldsymbol{x}} + \overline{\boldsymbol{B}}\, \boldsymbol{v} + \boldsymbol{L}(\psi)\, (\tilde{\boldsymbol{y}} - \hat{\boldsymbol{y}}) \\ \hat{\boldsymbol{y}} = \boldsymbol{C}\, \hat{\boldsymbol{x}} \end{cases} \tag{16}$$

where $\hat{\boldsymbol{x}} \triangleq \left[\hat{\boldsymbol{\eta}}^T, \hat{\boldsymbol{\nu}}^T\right]^T$ is the estimated state vector, $\boldsymbol{v} \triangleq \boldsymbol{u}_{\boldsymbol{PID}} + \boldsymbol{u}_{\boldsymbol{FF}}$ is the control vector, $\hat{\boldsymbol{y}} \equiv \boldsymbol{x}$ is the output vector that actually feeds the control system in Section 3, and $\tilde{\boldsymbol{y}} \in \mathbb{R}^8 \,|\, \tilde{\boldsymbol{y}} \triangleq \left[\tilde{\boldsymbol{\eta}}^T, \boldsymbol{0}^T\right]^T$ is the measurement vector, where $\tilde{\boldsymbol{\eta}} \in \mathbb{R}^4 \,|\, \tilde{\boldsymbol{\eta}} \equiv \boldsymbol{y}$ represents the measurements of position and heading angle of the ROV in Section 3. The matrices $\overline{\boldsymbol{A}(\psi)}$ and $\overline{\boldsymbol{B}}$ are the same as in (3), yet composed of $\overline{\boldsymbol{D}_{\boldsymbol{L}}}$ and $\overline{\boldsymbol{M}}$ instead of $\boldsymbol{D}_{\boldsymbol{L}}$ and $\boldsymbol{M}$, $\boldsymbol{C} \equiv \boldsymbol{I}$ (identity matrix of order 8), and the output injection matrix $\boldsymbol{L}(\psi)$ is defined as

$$\boldsymbol{L}(\psi) \triangleq \begin{bmatrix} \epsilon^{-1} \left(\overline{\boldsymbol{M}}\right)^{-1} & \boldsymbol{0} \\ \epsilon^{-2} \left(\overline{\boldsymbol{M}}\right)^{-1} \boldsymbol{J}^T(\psi) & \boldsymbol{0} \end{bmatrix} \tag{17}$$

where $\epsilon \in \mathbb{R}_{>0} \,|\, 0 < \epsilon \ll 1$ is the only tuning parameter.

The estimation error dynamics is given by

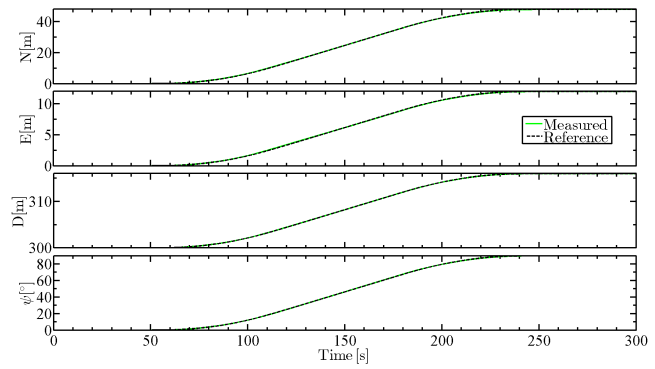

Fig. 1. Motion in the NED coordinate frame, where N = North, E = East, D = Down, and ψ = Heading angle.

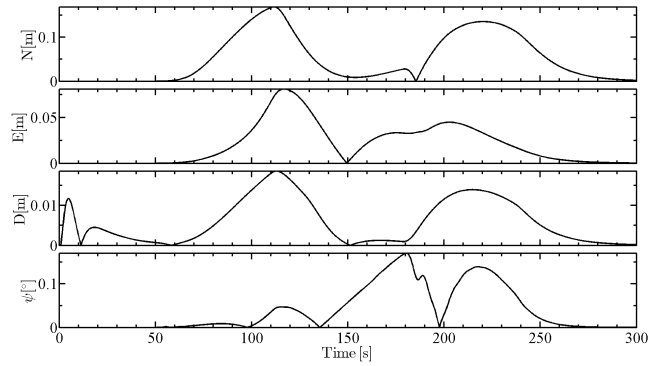

Fig. 2. Absolute position and heading tracking errors.

$$\dot{\boldsymbol{e}}_{\boldsymbol{e}} = \left(\overline{\boldsymbol{A}(\psi)} - \boldsymbol{L}(\psi)\,\boldsymbol{C}\right)\boldsymbol{e}_{\boldsymbol{e}} + \overline{\boldsymbol{B}}\,\boldsymbol{v} + \boldsymbol{L}(\psi)\,\tilde{\boldsymbol{y}} \qquad (18)$$

where the purely kinematic nonlinearities $\boldsymbol{J}(\psi)$ and $\boldsymbol{J}^T(\psi)$ in (18) do not affect the eigenvalues of the dynamic matrix $\boldsymbol{A}_{\boldsymbol{e}}(\psi) \triangleq \overline{\boldsymbol{A}(\psi)} - \boldsymbol{L}(\psi)\,\boldsymbol{C}$, as already discussed in Section 3. Thus, ϵ has to be chosen in a way $\boldsymbol{A}_{\boldsymbol{e}}(\psi)|_{\psi\equiv 0}$ is Hurwitz, as $\boldsymbol{J}(0) = \boldsymbol{J}^T(0) = \boldsymbol{I}$ is imposed for tuning purposes. The stability of the origin of (18) is assessed by the application of the Lyapunov's direct method with a suitable LFC. The amplitudes of the peaks tend to ∞, and their durations tend to zero, as $\epsilon \to 0$. However, in practice, the gains only need to be sufficiently high, not ∞. Thus, $\epsilon \not\to 0$, due to several limiting factors, e.g. trade-off between the estimation accuracy and system bandwidth (Khalil, 2002; Atassi and Khalil, 2000). The tuning is thus properly made by choosing ϵ small enough to guarantee accurate estimation without over-broadening the frequency bandwidth to avoid that excessive measurement noise comes in, contaminating the system's response. As the estimation peaks, the control vector peaks consequently. To secure that the controller is never overreacting to the peaks, and possibly jeopardising the stability of the output feedback system, the control vectors $\boldsymbol{u}$ and $\boldsymbol{v}$ have to be saturated, as suggested in Khalil (2002). Yet, saturation is rather a natural feature, since the ROVs' propulsion systems have limited capacity and nonzero response time. Therefore, the vector $\boldsymbol{v}$ has to saturate at the most at the limits of the propulsion system.

5. SIMULATION RESULTS

The ROV Minerva started being run in DP (Dynamic Positioning) at the initial position $p_i = (0, 0, 300)$ [m], then traversed a 52 m-long straight line path from p_i to the final position $p_f = (48, 12, 316)$ [m], while changing the heading angle from $\psi_i = 0°$ at p_i to $\psi_f = 90°$ at p_f, and lastly remained in DP at p_f. The transect was taken at relatively high speed, given Minerva's ratings, to arouse the couplings among all DoFs to challenge the MCS. The sea current was set to zero, such that $\boldsymbol{c} = \boldsymbol{0}$, and there also was random plant parameter variation in the simulation.

Table 1. Summary of information in Figs. 1–2.

DoF	Absolute error	Mean error	Standard dev.[1]
N	$\leqslant 0.169$ m (@111.60 s)	0.000 m	0.150 m
E	$\leqslant 0.081$ m (@116.80 s)	0.000 m	0.060 m
D	$\leqslant 0.019$ m (@113.00 s)	0.000 m	0.020 m
ψ	$\leqslant 0.170°$ (@180.40 s)	0.000°	0.130°

[1]: Assuming normal (or Gaussian) distributions for the errors.

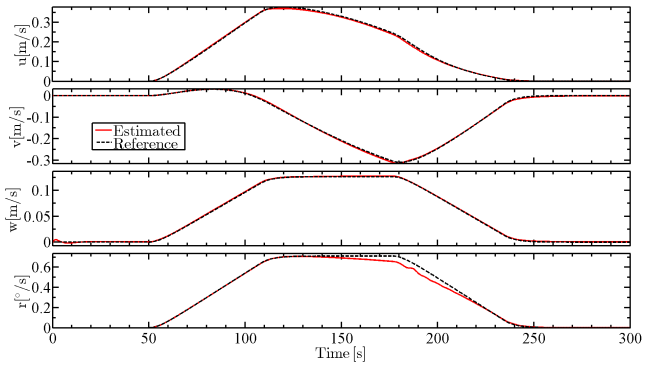

Fig. 3. Estimated linear velocities and yaw rate.

Fig. 1 depicts the motion along the reference path decomposed componentwise. Fig. 2 depicts the absolute position tracking errors. Table 1 summarises the information in both figures. The standard deviations (assuming normal distribution) show that the position and heading tracking errors were acceptably small. Both figures show that the motion was smooth enough to allow successful video-based survey missions to be carried out. The initial peak was not too pronounced, and took a relatively long time to vanish, due to the fact that the gains of the HGSO were just sufficiently high for this application. Yet, they were $< \infty$.

Fig. 3 depicts the estimated velocities and a comparison against the velocity references. The discrepancy between both sets were larger for higher velocities, as it could already be expected, since the modelling uncertainties are typically accentuated at higher velocities. As a consequence, the mismatch between the version of the CPM that is mimicked by the HGSO and the version of the CPM whose dynamics is linearised through the use of the term $\boldsymbol{u}_{\boldsymbol{LIN}}$ increases at higher velocities. Nonetheless, the estimation was fairly accurate and fulfilled its purpose of supplying the MIMO PID controller with the filtered state vector. The initial peak did not destabilise the MCS.

Fig. 4 shows the commanded thrust forces. None of the propellers was commanded to work in saturation. Under saturation, the performance of the MCS could be more or less severely affected depending on the duration of the saturation period and the intensity of the disturbances acting on the ROV. The MCS would remain stable under saturation, though. The figure also indicates that the MCS made good use of energy and avoided unnecessary wear and tear of the thrusters, since a tight reference tracking was achieved (Fernandes et al., 2012).

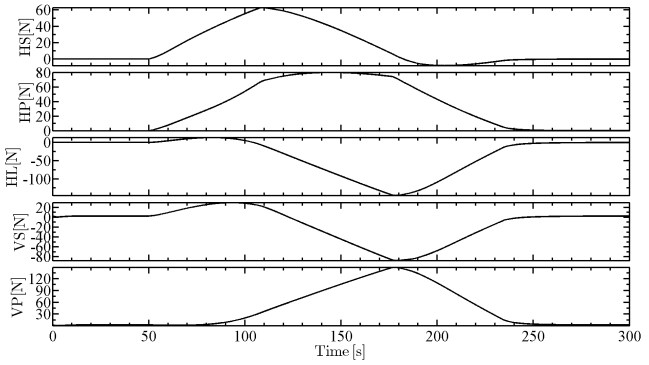

Fig. 4. Commanded thrust forces, where the letters H = Horizontal, V = Vertical, S = Starboardside, P = Portside, and L = Lateral help in identifying the five propellers within the structure of the ROV Minerva.

6. CONCLUDING REMARKS

The proposed output feedback motion control system achieved satisfactory reference tracking performance in simulations under challenging operating conditions. The results presented in this work encourage full-scale trials at sea to be carried out as a natural continuation, in order to confirm, and possibly extend, the simulated results.

ACKNOWLEDGEMENTS

The present result is part of the work carried out at AMOS (Centre for Autonomous Marine Operations and Systems) and at AUR-Lab (Applied Underwater Robotics Laboratory). The Norwegian Research Council is acknowledged as the main sponsor of this work.

REFERENCES

Åström, K.J. and Hägglund, T. (2011). *PID controllers: theory, design, and tuning*. Instrument Society of America, North Carolina, 2nd edition.

Atassi, A.N. and Khalil, H.K. (2000). Separation results for the stabilization of nonlinear systems using different high-gain observer designs. *International Journal of Control*, 39(3), 183–191.

Breivik, M. and Fossen, T.I. (2009). Guidance laws for autonomous underwater vehicles. In A.V. Inzartsev (ed.), *Underwater Vehicles*, chapter 4, 51–76. I-Tech, Vienna, Austria.

Caccia, M., Indiveri, G., and Veruggio, G. (2000). Modeling and identification of open-frame variable configuration unmanned underwater vehicles. *Journal of Oceanic Engineering*, 25(2), 227–240.

Christ, R.D. and Wernli, R.L. (2007). *The ROV manual: a user guide for observation class remotely operated vehicles*. Butterworth-Heinemann, Oxford, UK.

Esfandiari, F. and Khalil, H.K. (1992). Output feedback stabilization of fully linearizable systems. *International Journal of Control*, 56(5), 1007–1037.

Estrada, M.B., Garcia, M.F., Malabre, M., and García, J.C.M. (2007). Left invertibility and duality for linear systems. *Linear Algebra and Its Applications*, 425(2–3), 345–373.

Fernandes, D.A., Dukan, F., and Sørensen, A.J. (2012). Reference model for high performance and low energy consumption motions. In *IFAC NGCUV 2012 – Portugal*, 217–222.

Fossen, T.I. (2011). *Handbook of marine craft hydrodynamics and motion control*. John Wiley & Sons, Ltd., Chichester, UK.

Franklin, G.F., Powell, J.D., and Emami-Naeini, A. (2009). *Feedback control of dynamic systems*. Prentice Hall, Inc., Upper Saddle River, 6th edition.

Kailath, T. (1980). *Linear systems*. Prentice Hall, Inc., Upper Saddle River.

Khalil, H.K. (2002). *Nonlinear systems*. Prentice Hall, Inc., Upper Saddle River, 3rd edition.

Lewandowski, E.M. (2004). *The dynamics of marine craft: maneuvering and seakeeping*, volume 22 of *Advanced Series on Ocean Engineering*. World Scientific Pub., Arlington.

Ludvigsen, M., Sortland, B., Johnsen, G., and Singh, H. (2007). Applications of geo-referenced underwater photomosaics in marine biology and archaeology. *Oceanography*, 20(4), 140–149.

Marsh, L., Copley, J.T., Huvenne, V.A.I., Tyler, P.A., and the Isis ROV Facility (2013). Getting the bigger picture: using precision remotely operated vehicle (ROV) videography to acquire high-definition mosaic images of newly discovered hydrothermal vents in the southern ocean. *Deep Sea Research Part II: Topical Studies in Oceanography*. In Press.

Perrier, M. and Canudas-de-Wit, C. (1996). Experimental comparison of PID vs. PID plus nonlinear controller for subsea robots. *Autonomous Robots*, 3(2), 195–212.

Singh, H., Roman, C., Pizarro, O., Eustice, R., and Can, A. (2007). Towards high-resolution imaging from underwater vehicles. *The International Journal of Robotics Research*, 26(1), 55–74.

Slotine, J.J.E. and Li, W. (2005). *Applied nonlinear control*. Pearson Education Taiwan Ltd., Taipei, Taiwan.

SNAME (1950). The Society of Naval Architects and Marine Engineers. nomenclature for treating the motion of a submerged body through a fluid. In *Technical and Research Bulletin*, 1–5.

Sørensen, A.J. (2013). *Marine control systems: propulsion and motion control of ships and ocean structues*. Lecture notes. Marine Technology Centre, Trondheim, Norway, 3rd edition.

Sørensen, A.J., Dukan, F., Ludvigsen, M., Fernandes, D.A., and Candeloro, M. (2012). Development of dynamic positioning and tracking system for the ROV Minerva. In G.N. Roberts and R. Sutton (eds.), *Further Advances in Unmanned Marine Vehicles (IEE Control Eng. Series – Volume 77)*, chapter 6, 113–128. IEE – The Institution of Electrical Engineers, Stevenage, UK.

Appendix A. NTNU'S ROV MINERVA

Minerva is a SUB-fighter 7500 ROV made by Sperre AS in 2003 for NTNU. The NTNU's R/V (Research Vessel) Gunnerus (http://www.ntnu.edu/marine/gunnerus) is the support vessel used to carry out operations with Minerva. The ROV is powered from, and communicates with, R/V Gunnerus via a 600 m-long umbilical cable. It has five thrusters with fixed pitch propellers. A high-precision acoustic positioning system HiPAP 500 by Kongsberg measures the ROV's position relative to R/V Gunnerus. The MCS is implemented on a cRIO, and programmed via LabVIEW, both by National Instruments.